ABOUT IJPS

The **International Journal of Physical Sciences (IJPS)** is published weekly (one volume per year) by Academic Journals.

International Journal of Physical Sciences (IJPS) is an open access journal that publishes high-quality solicited and unsolicited articles, in English, in all Physics and chemistry including artificial intelligence, neural processing, nuclear and particle physics, geophysics, physics in medicine and biology, plasma physics, semiconductor science and technology, wireless and optical communications, materials science, energy and fuels, environmental science and technology, combinatorial chemistry, natural products, molecular therapeutics, geochemistry, cement and concrete research, metallurgy, crystallography and computer-aided materials design. All articles published in IJPS are peer-reviewed.

Contact Us

ARTICLES

Full Length Research Paper

Electrical resistivity and Seebeck coefficient of $Pd_{81}Ge_{19}$

A. Achouri*, A. Boukraa and L. Mohammedi

Université d'Ouargla, Faculté des Mathématiques et des Sciences de la Matière, Lab. Développement des énergies nouvelles et renouvelables dans les zones arides et sahariennes, Ouargla 30000, Algeria.

We report on the simultaneous measurement of resistivity and Seebeck coefficients in samples of $Pd_{81}Ge_{19}$ ribbons prepared by the melt spinning technique method and having a typical dimension of 40.0 mm × 1.75 mm × 0.028 mm. The investigation was performed using a new completely automated device in a large temperature range (from room to 700°C). Structural changes, crystallization times and heat treatments on several samples of the same composition were followed as a function of temperature. Seebeck coefficients, reported for the first time in these samples, varied roughly between -2 and -21 µV/K in the temperature range of 25 to 700°C, while the electrical resistivity varied roughly between 35 and 120 µΩ.cm in agreement with the literature. Complementary differential scanning calorimetry (DSC) and scanning electron microscopy (SEM) experiments were also carried out and confirm the phase transitions observed by the above mentioned techniques.

Key words: Seebeck coefficient, melt spinning technique, crystallization temperature, electrical resistivity, phase transitions.

INTRODUCTION

Crystallization kinetics of metallic glasses have been studied for many years (Calvo-Dahlborg et al., 1997) and they continue to be an attractive field because of their interesting properties for industrial applications. The physical properties depend on their chemical composition and production process (Calvo-Dahlborg et al., 2011). Among their cited properties are electrical resistivity and Seebeck coefficient, which are directly related to the atomic structure and the coupling between them can often be used to characterize the electrical conduction mechanisms in solids (Dordor et al., 1980; Mott and Davis, 1971). They are sensitive to structural, magnetic and alloying phase transformations. Measurements of the electrical resistivity and Seebeck coefficient allow a better

understanding of electrical properties of amorphous alloys. It is well-known that they can be used to study the kinetics of crystallization during thermal processes or other structural changes such as particle growth. The Pd-Ge amorphous alloy is among the most studied systems. It can be amorphous for a large Germanium content. Few studies concerning crystallization of $Pd_{81}Ge_{19}$ amorphous alloys were performed by other techniques. Budhani et al. (1983) studied the variation of the resistivity as a function of temperature for $Pd_{80}Ge_{20}$ and $Pd_{77.5}Ge_{22.5}$ continuously heated at 10°C/min through the temperature range 300 to 710 K. They observed that the crystallization process starts around 600 and 550 K respectively in a direct transformation. They also found that the electrical

resistivity for the $Pd_{80}Ge_{20}$ alloy is greater than 100 µΩcm. The diffraction pattern of the $Pd_{80}Ge_{20}$ ribbon at room temperature is characterized by two broad intensity peaks at 2θ = 40° and 72° (Budhani et al., 1983).

The aim of this paper is to present thermoelectric properties for an amorphous palladium-based alloy ribbon, $Pd_{81}Ge_{19}$, using a new completely automated device which measures simultaneously the resistivity and the Seebeck coefficient for liquid and amorphous conductors. Structural changes were followed as a function of temperature (from room temperature to 700°C), crystallization time and heat treatments on several samples of the same composition $Pd_{81}Ge_{19}$.

EXPERIMENTAL METHODS

Electrical resistivities and Seebeck coefficients are very sensitive to any structural change, and amorphous samples are a good example to assess the capability of our apparatus to determine crystallization temperatures and identify structural changes. If the change is not especially manifest in one property, it is hoped that it will be in the second one. It is therefore important to measure simultaneously these two properties. Measurements were obtained using an automated device developed and continuously improved for several years in the LCP-A2MC laboratory (Metz, France), which measures jointly (that is, simultaneously) or separately the electrical resistivity and the Seebeck coefficient. The electrical resistivity is measured using a four probes DC standard technique and the Seebeck coefficient using a small variation of temperature (around the measurement temperature) as described by Abadlia et al (2014). We measure the voltage between the same wire (V_{13} and V_{24}) when the temperature of one of the junctions varies from T-ΔT to T+ΔT (ΔT can vary from 1 to 6°C). The Seebeck coefficient (Absolute Thermoelectric Power) is given by the formula (Gasser, 2000):

$$S = \frac{S_{AB}}{p-1} + S_A \qquad (1)$$

Where S_{AB} and S_A are respectively the Seebeck coefficient of a thermocouple AB and the Seebeck coefficient of an element A and p is the slope of thermoelectric power as a function V_{24}/V_{13} which does not depend on spurious voltages or drift.

The experimental device and a LabVIEW software allow measurements in the temperature range -200 to 1330°C using any type of standard thermocouple. The sample is placed into a quartz tube connected to a vacuum pump and argon gas to avoid oxidation at high temperature. Two K-type thermocouples are used (whose calibration polynomials exist in the NIST tables) (Standard, 1995) to measure temperature (within 1% error) and different voltages for resistivity and Seebeck coefficient. Connections between sample and thermocouples are realised using stainless connectors. A temperature difference between the junctions is created using a heater controlled by the software. Two other K-type thermocouples are used to control temperature inside the furnace and give the operator an idea about how to position the furnace to insure temperature homogeneity. The general description of the experimental setup is described in the work of Abadlia *et al* (2014). For this work, the resistivity and the Seebeck coefficient have been measured between room temperature and 700°C (at this latter temperature, close to the fusion temperature, we might assert that crystallisation is complete and we do not need to heat the sample

any more), both by increasing then by decreasing temperature. The heating and cooling rate is 0.3°C per minute in order ascertain permanent thermal equilibrium between the system and the furnace (quasi-static regime).

Resistivity measurements are relatively simple even though our experimental setup requires the precise knowledge of sample geometry. For amorphous ribbons, the length and the width are easy to determine but thickness is too small to be determined with reasonable precision (20 µm) in addition to being not constant along the sample. For these reasons, we prefer to present measurements relative to the room temperature resistivity value. Measurements of Seebeck coefficients are more complicated than those of resistivity but one does not need the knowledge of geometry and the result is in absolute value.

Our samples are $Pd_{81}Ge_{19}$ ribbons which were prepared by the melt spinning technique method (Liebermann and Graham, 1976) with a typical dimension of 40.0 mm × 1.75 mm × 0.028 mm.

RESULTS AND DISCUSSION

In this work, we have measured the resistivity and the Seebeck coefficient for $Pd_{81}Ge_{19}$, as a function of temperature. Resistivity and Seebeck coefficient are measured simultaneously at exactly the same time, in the same sample under the same conditions. One of the measured quantities might change while the other remains constant. Therefore, it is important to measure the two properties for the same sample and the same time.

Resistivity and the Seebeck coefficient as a function of temperature

Continuous resistivity and Seebeck coefficient measurement curves show a drastic and important change before the melting temperature is reached characteristic of a behaviour which occurs in amorphous phases. When heated, the amorphous material crystallizes and a marked change is observed in resistivity and Seebeck coefficient curves corresponding to crystallization temperatures.

We report in Figures 1 and 2 relative resistivity and Seebeck coefficient measurements for amorphous and crystallised $Pd_{81}Ge_{19}$ with respect to temperature. The resistivity increases slightly from 117 µΩ.cm at room temperature up to 120 µΩ.cm at 270°C where we see clearly a sharp bend between 270 and 300°C. Then, we notice a first phenomenon consisting of a rapid decrease from the value 117 µΩ.cm down to 68 µΩ.cm between 300 and 360°C before stabilizing then increasing slightly between 370 and 440°C. Next, the resistivity continues its slight increase up to 74.5 µΩ.cm at 470°C, where it is found that the second phenomenon is completed. The augmentation of resistivity is enhanced between 470 and 625°C (from 74.5 to 87.5 µΩ.cm). A third downward transition begins at 625°C and persists up to 640°C (from 87.5 to 81 µΩ.cm). Once heated at 685°C, the curves of second heating and second cooling of the sample
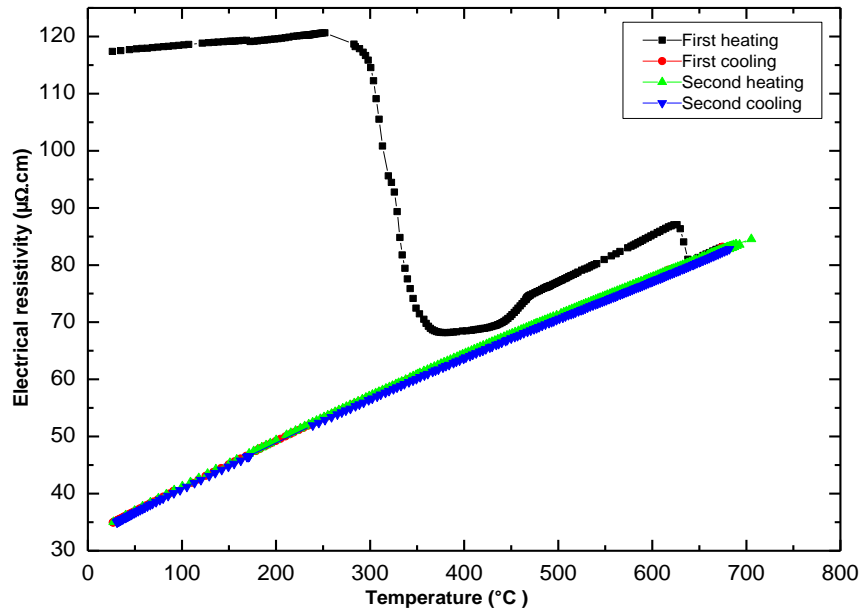
Figure 1. Electrical resistivity of $Pd_{81}Ge_{19}$ as a function of temperature.
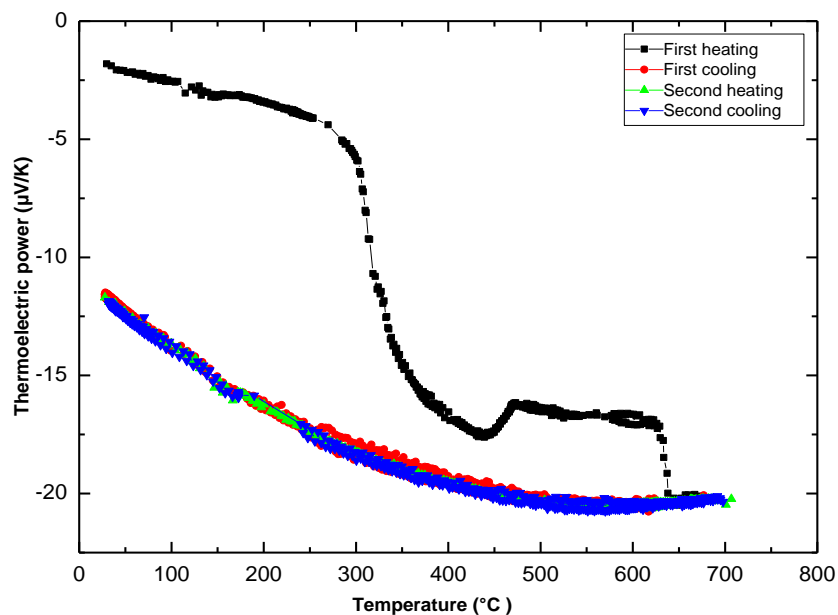
Figure 2. Seebeck coefficient of $Pd_{81}Ge_{19}$ as a function of temperature.

become superposed with the first cooling one and there is no more change in the resistivity curve. The linear increase of resistivity with temperature (from ambient to 700°C) is indicative of a metallic nature for $Pd_{81}Ge_{19}$.

For the Seebeck coefficient, we can observe that the starting value -2 µV/K is negative when $Pd_{81}Ge_{19}$ is amorphous, where it decrease slightly with increasing temperature, then starts bending like the resistivity between 260 and 300°C, before decreasing abruptly from

-7 µV/K at about 300°C to -15 µV/K at about 360°C. It continues to decrease but less steeply beginning at 360°C, passes through a minimum at -17.5 µV/K at 440°C and then increases slightly to -16.25 µV/K at 470°C. It stabilizes to approximately -16.5 µV/K in the interval 470 to 625°C. We can observe a third transition beginning from -17 µV/K at 625°C to -20 µV/K at 640°C and above. The first cooling and the second heating/ cooling of temperature give superimposed curves in the
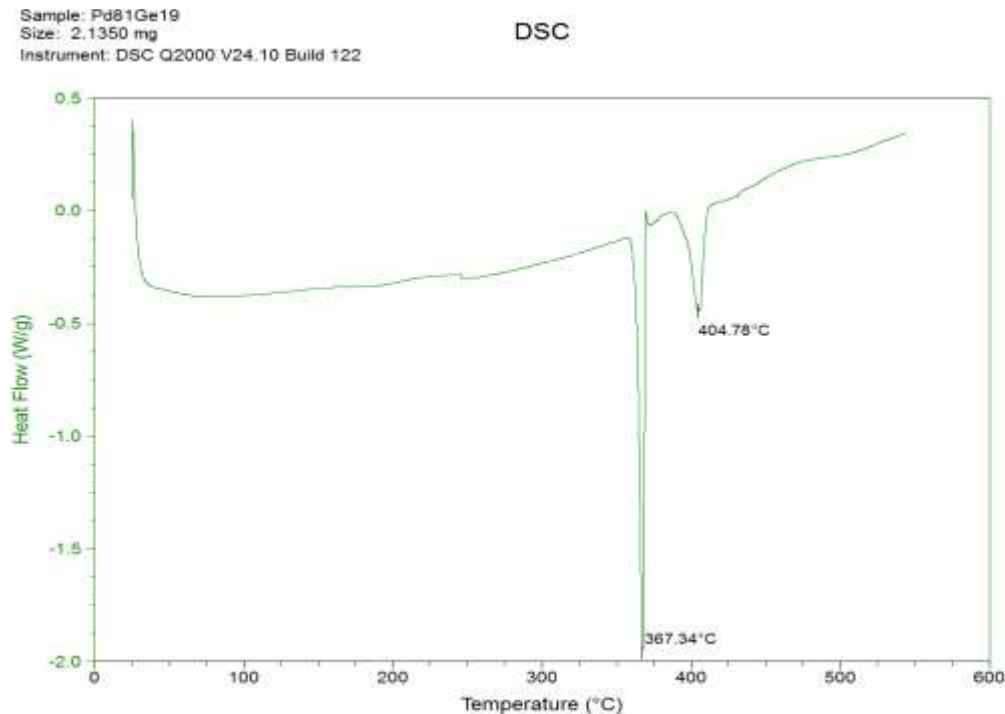
Figure 3. DSC trace of $Pd_{81}Ge_{19}$.

whole temperature range and no more changes are observed. It is interesting to remember that the two properties are measured simultaneously on the same sample. Between 300 and 450°C, resistivity and Seebeck coefficient changes are very important (The first from 120 to 70 µΩ.cm and the second from -6 to -17.5 µV/K). This shows that these two properties are complementary and resistivity measurements alone cannot give all information about crystallization kinetics.

Characterization techniques: DSC and SEM

DSC analysis

Phase transformations (or transitions) in matter can be followed by measuring some physical properties as a function of a given thermodynamic property such as temperature, pressure, etc. In this way, a simple technique called Differential Scanning Calorimetry (DSC) can be used to realise such kind of measurements. In general, it has the advantage of both simplicity and low cost but our apparatus had also the limitation of a minimal rate of 5°C/mn which is too high compared to the 0.3°C/mn rate used in the resistivity and ATP measurements. A lower rate would ordinarily produce larger measurement peaks. In addition, DSC cannot follow transformations as a function of time at constant temperature. The DSC experiment was performed on our $Pd_{81}Ge_{19}$ sample revealing a large transition at 367.34°C,

and a second at 404.78°C. A representative DSC curve of the $Pd_{81}Ge_{19}$ ribbon is shown in Figure 3. Comparing the DSC results to the electrical resistivity and thermoelectric power ones, the same phase transitions can be seen at about the same temperatures.

SEM observations

Scanning Electron Microscopy (SEM) and Transmission Electron Microscopy (TEM) can also give topology of the surface and determine its structure. But these techniques have some inconveniences: (i) Their cost is very high (expensive); (ii) They must be supervised by a dedicated operator; (iii) they cannot follow the continuous evolution of the material as a function of temperature and the measurement must be done at a constant one.

The surface morphology of our sample $Pd_{81}Ge_{19}$ was determined by SEM (Li et al., 1998; Maeda and Mater, 1994). According to the SEM picture in Figure 6, the $Pd_{81}Ge_{19}$ amorphous alloy is comprised of thousands of small particles distributed homogeneously on the surface. According to Figures 4 and 5, we cannot observe any anomalous features on the two types of ribbon surfaces which leads us to believe that our sample is in an amorphous phase at room temperature. From 400°C, just after the first phase transition, the crystal grains were observed on the thermal treatment generated matt and shiny sides of $Pd_{81}Ge_{19}$, indicating the onset of crystallization at this temperature (Figures 6 and 7). At
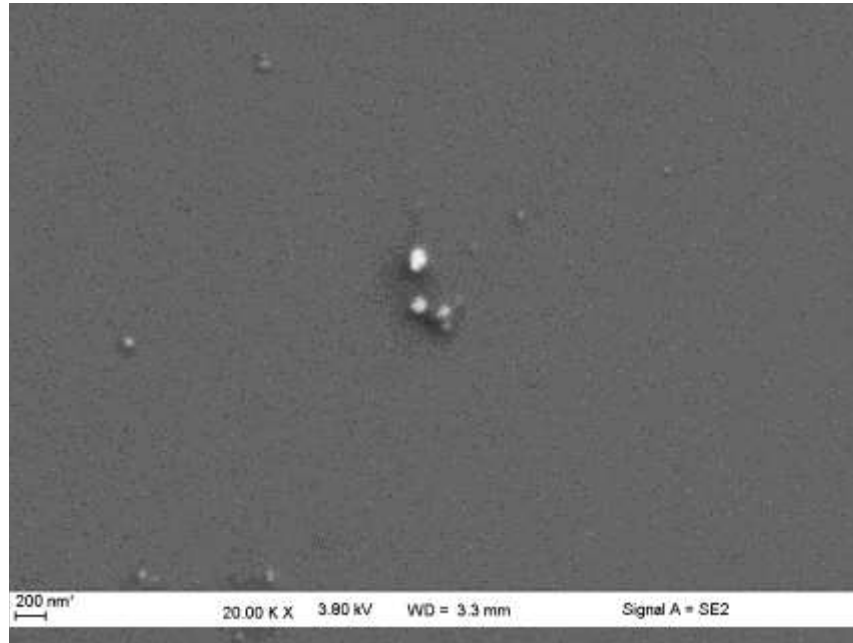
Figure 4. Scanning electron micrograph of $Pd_{81}Ge_{19}$, shiny side at room temperature.
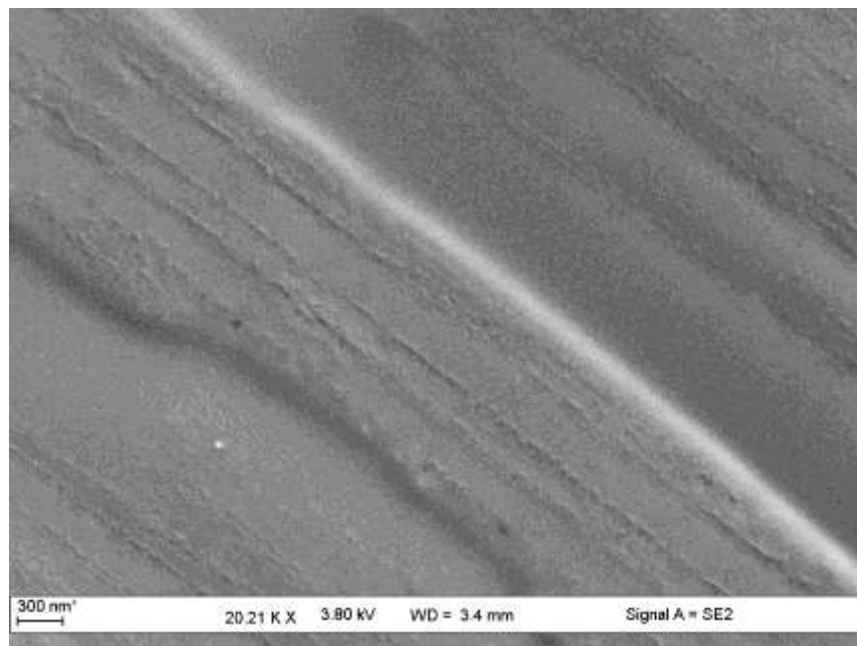
Figure 5. Scanning electron micrograph of $Pd_{81}Ge_{19}$, Matt face at room temperature.

500°C, we observe clearly the formation of crystal grains on both bright and matt sides of our ribbon (Figures 8 and 9).

Finally, the crystal grains enlarge gradually up to 600°C, indicating that crystallization was essentially complete at 600°C (Figures 10 and 11). Preliminary X-ray diffraction results , not shown here, indicate the presence of a two-phase mixture of $Pd_{25}Ge_9$ and Pd_5Ge in these samples in partial agreement with published results by Nava et al. (1981) who observed only $Pd_{25}Ge_9$ (as well as
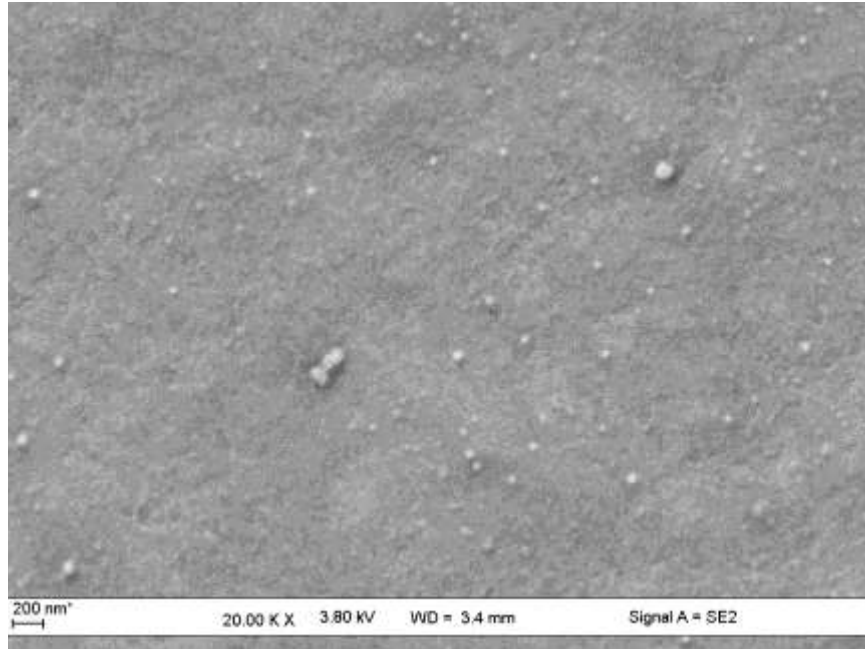
Figure 6. Scanning electron micrograph of $Pd_{81}Ge_{19}$, Shiny side at 400°C.
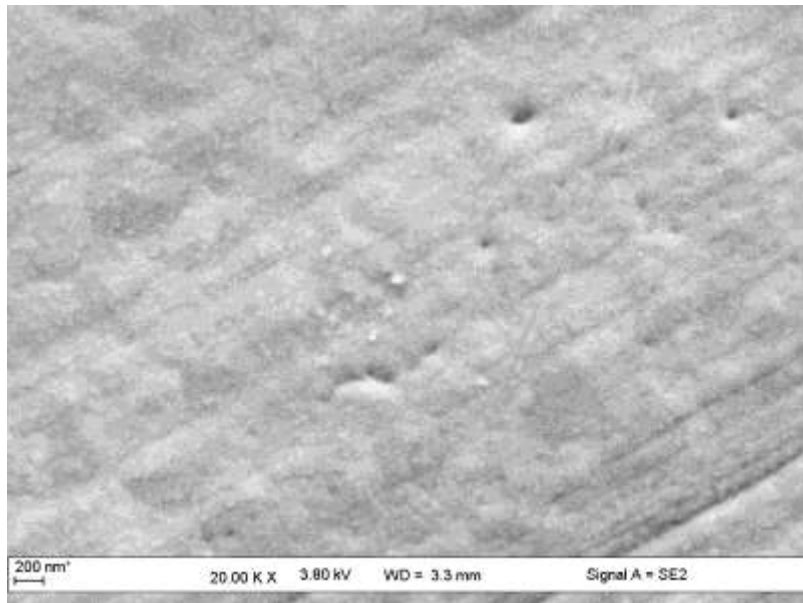
Figure 7. Scanning electron micrograph of $Pd_{81}Ge_{19}$, Matt face at 400°C.

α-Pd) and with Khalaff and Schubert (1974) who detected only the Pd_5Ge (as well as Pd_3Ge) phases.

Conclusion

We have performed precise and reproducible simultaneous measurements of electrical resistivity and Seebeck coefficient in a large temperature range by means of an automated device. Measurements were made as a function of temperature and time. Resistivity and Seebeck coefficient are very sensitive to structural changes and amorphous samples are illustrative of these amorphous-crystalline transformations and their
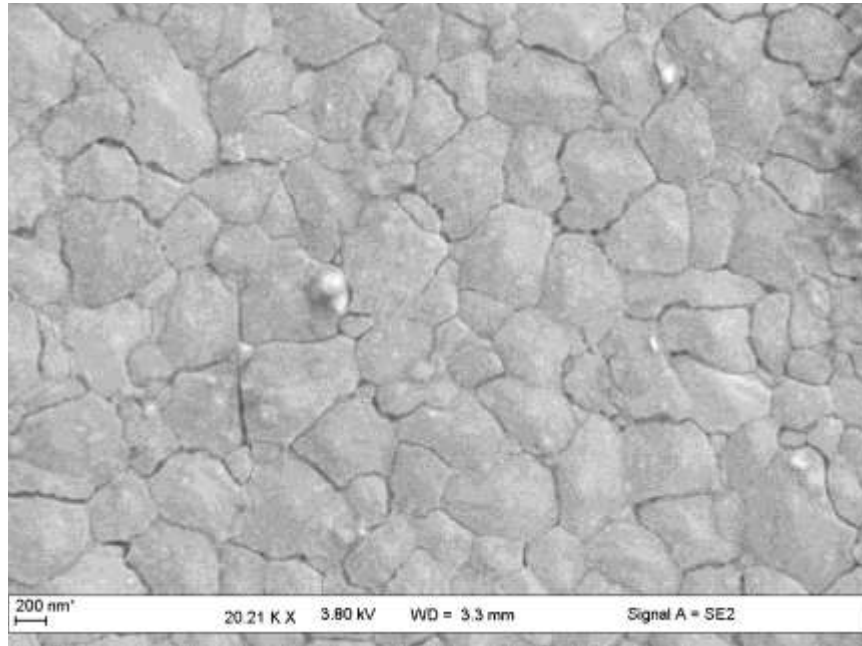
Figure 8. Scanning electron micrograph of Pd81Ge19, Shiny side at 500°C
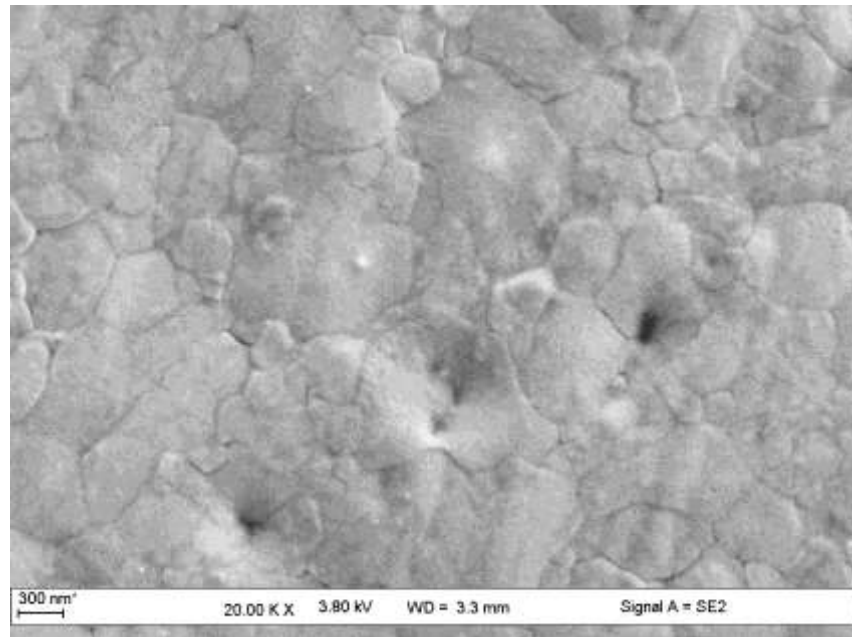
Figure 9. Scanning electron micrograph of $Pd_{81}Ge_{19}$, Matt face at 500°C.

characteristic crystallization temperatures. It is reported in this paper that the Seebeck coefficients of the samples vary between approximately -2 µV/K when $Pd_{81}Ge_{19}$ is amorphous to -21 µV/K when crystallization is complete (in the temperature range from 25 to 700°C). Afterwards, a third transition begins starting from -17 µV/K at 625°C

down to -20 µV/K at 640°C and above. At the same time, the electrical resistivity diminishes approximately from 120 µΩ.cm (when $Pd_{81}Ge_{19}$ is amorphous) to 35 µΩ.cm (when crystallization has completed) in agreement with the literature. Measurement of resistivity and Seebeck coefficient as a function of temperature or time gives
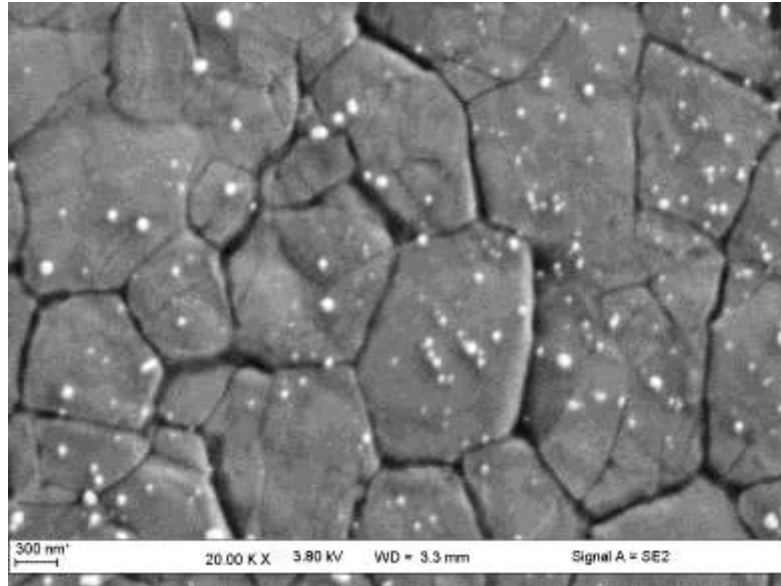
Figure 10. Scanning electron micrograph of $Pd_{81}Ge_{19}$, Shiny side at 600°C
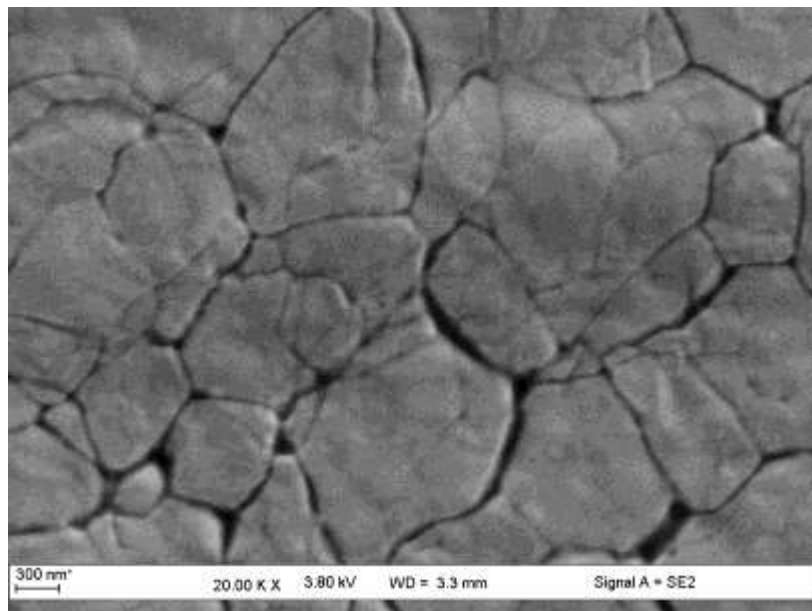
Figure 11. Scanning electron micrograph of $Pd_{81}Ge_{19}$, Matt face at 600°C.

complementary information about the kinetics of crystallization processes. As supplementary techniques, we completed the above results by using the DSC and SEM/TEM tools in the investigation of the kinetics and morphology of these crystalline-amorphous transitions.

Conflict of Interests

The authors have not declared any conflict of interests.

REFERENCES

Abadlia L, Gasser F, Khalouk K, Mayoufi M, Gasser JG (2014). New experimental methodology, setup and LabView program for accurate

absolute thermoelectric power and electrical resistivity measurements between 25 and 1600 K: Application to pure copper, platinum, tungsten, and nickel at very high temperatures. Rev. Sci. Instruments 85(9):095121.

Budhani RC, Goel TG, Chopra KL (1983). Transformation behaviour of the metastable phases in rapidly solidified Pd-Ge alloys. J. Mater. Sci. 18:571-581.

Calvo-Dahlborg M, Dahlborg U, Ruppert JM (2011). Influence of superheat before quench on the structure and stability of NiP metallic glasses studied by neutron scattering techniques. J. Non Cryst. Solids 357:798-808.

Calvo-Dahlborg M, Machizaud F, Nhien S, Vigneron B, Dahlborg U (1997). Structural study of a phase transition in a NiP metallic glass. Mater. Sci. Eng. A, 226:197-203.

Dordor P, Marquestaut E, Villeneuve G (1980). Dispositif de mesures du pouvoir thermoélectrique sur des échantillons très résistants entre 4 et 300 K. Rev. Phys. Appl. 15:1607-1612.

Gasser JG (2000). Contribution à l'étude des propriétés électroniques, résistivité et pouvoir thermoélectrique, d'alliages de métaux polyvalents et de transition à l'état liquide (Ge-Sb, Pb-Sb, Mn-Sb, Mn-Sn, Mn-In, et Mn-Zn). PhD Dissertation, University of Metz.

Khalaff K, Schubert K (1974). Constitution of the Pd-Ge System. Z Metallkunde 65:379-382.

Li H, Chen HS, Dong S, Yang J, Deng JF (1998). Study on the crystallization process of Ni-P amorphous alloy. Appl. Surface Sci. 125:115-l19.

Liebermann HH, Graham Jr. CD (1976). Production of amorphous alloy ribbons and effects of apparatus parameters on ribbon dimensions, Magnetics. IEEE Trans. Magnetics 12:921-923.

Maeda K, Mater J (1994). Crystallization mechanism of amorphous $Ni_{65}Cr_{16}P_{19}$ metallic alloys. J. Mater. Sci. 29:1449-1454.

Nava F, Majni G, Ottaviani G, Galli E (1981). Compound formation kinetics in the Si/Pd and Ge/Pd systems. Thin Solid films 77:319.

Mott NF, Davis EA (1971). Electronic processes in non-cristalline materials, Clarendon Press, Oxford.

Standard (1995). A. S. T. M. Annual Book of American society for Testing and Material, General Methods and Instrumentation. Temp. Meas. 14:14.

Full Length Research Paper

Natural radioactivity level of clay, ceramic, and stone cooking dishes in Saudi Arabia

Alharbi W. R.

Department of Physics, Faculty Science, King Abdulaziz University, Jeddah, Saudi Arabia.

Standards and guidelines are needed in the manufacture of household cooking dishes from clay, ceramic, and stone in Saudi Arabia. The radioactivity levels due to the presence of ^{40}K, ^{232}Th, and ^{226}Ra in these materials were determined using gamma spectrometry equipped with high purity germanium (HPGe) detector. The activity concentrations of ^{226}Ra ranged from 5.75 Bq kg^{-1} (Yemen stone sample) to 192.35 Bq kg^{-1} (China ceramic sample), those of ^{232}Th ranged from 6.17 Bq kg^{-1} (Yemen stone sample) to 192.41 Bq kg^{-1} (China ceramic sample), and those of ^{40}K ranged from 43.92 Bq kg^{-1} (clay sample manufactured in Bahrah, Saudi Arabia) to 656.96 Bq kg^{-1} (ceramic sample from Romania). Radiological indices were measured for all samples to ascertain the potential radiation health hazards. The average concentrations for ^{226}Ra and ^{232}Th and the absorbed dose rate (D_R) in clay and ceramic dishes exceeded the permissible global limits, with the exception of clay samples from Makkah, Saudi Arabia. The ^{226}Ra and ^{232}Th concentrations in all cooking dishes manufactured from stone were within safety limits. However, most of the average values obtained for the activity concentration of ^{40}K exceeded the recommended limit. The radium equivalent (Ra_{eq}), annual gonadal dose equivalent (AEDE), external hazard index (H_{ex}), and gamma activity index (I_{γ}) were found to be below the internationally accepted safe limit, except in a ceramic sample imported from China. The sample also had an annual effective dose (AEDE) that slightly above unity. The concentrations of a total of 33 chemical elements were estimated by using an ARL QUANT'X energy-dispersive X-ray fluorescence spectrometer. In most samples, the elements' concentrations exceeded the reference level values. In conclusion, care must be taken when using cooking dishes manufactured from clay, ceramic, and stone.

Key words: Energy-dispersive X-ray fluorescence (EDXRF) analyzer, gamma spectrometry, radiation hazard, household cooking dishes, natural radioactivity.

INTRODUCTION

Daily exposure to the natural radionuclides ^{232}Th, ^{226}Ra, and ^{40}K is undesirable. They cause an internal exposure

risk resulting from radon and its decay products and an external exposure risk due to their gamma emission

(United Nations Scientific Committee on the Effect of Atomic Radiation [UNSCEAR], 2000; Amin and Naji, 2013). Chronic exposure to low doses of natural radioactivity can cause adverse health effects (Najam et al., 2015). The most serious involve increased probability of cancer and birth defects (Faisal et al., 2014).

Most household cooking dishes manufactured from clay, ceramic, and stone contain various concentrations of the natural radionuclides ^{226}Ra, ^{232}Th and ^{40}K. The precise concentrations depend on the chemical composition of the material, which is related to the geological conditions and geophysical characteristics of their origin (Salas et al., 2006). The materials may contain radionuclides from both natural sources and waste products in addition to some minerals from certain slags. The present study centers on radiological baseline information of the Jeddah region in particular and Saudi Arabia in general.

Many ways exist for analyzing trace elements in a material, including portable energy-dispersive X-ray fluorescence (EDXRF) spectrometry with radioisotope excitation. This method is useful and significantly reduces the number of samples needed for analysis (El-Taher, 2012; Sitko et al., 2004).

The aims of the present study were to analyze household cooking dishes manufactured from clay, ceramic, and stone (1) to determine the natural radionuclide levels using high-resolution gamma-ray (HPGe) spectrometry to evaluate the radiological risks and human exposure, and (2) to specify the concentrations of elements using EDXRF spectrometry.

MATERIALS AND METHODS

Sampling and sample preparation

A total of 20 samples of household cooking dishes used in Saudi Arabia were collected from local stores. Four samples were manufactured in Saudi Arabia, and the other 16 samples were imported from different foreign countries (Table 1). Each sample dish was crushed and sieved through a 1-mm mesh size to ensure homogeneity of the samples for testing. Weighted samples were placed in standard polyethylene beakers (650 cm^3 volume). The beakers were completely sealed and left for 4 to 5 weeks prior to gamma spectrometric analysis to attain secular equilibrium between radium, thorium, and their progenies products to ensure that radon gas was restricted to the beaker and the decay products remained in the sample (Hassan et al., 2010; Alharbi, 2013; Guidotti et al., 2015). For elemental analysis using EDXRF spectrometry (ARL QUANT'X EDXRF, Thermo Electron Corp., Middleton, WI), the dry samples (at room temperature) were crushed to a fine powder in an agate mortar, then sifted through a 0.25-mm sieve. The powder was then manually pressed into the sample holder, following the procedures described by Hartyàni et al. (2000).

Measurement of specific activity with gamma spectrometry

The specific activities of ^{226}Ra, ^{232}Th, and ^{40}K in the samples were

Table 1. Sample codes and countries of origin.

Sample code	Sample type	Country
D1	Clay	Egypt
D2	Clay	Pakistan
D3	Clay	Spain
D4	Clay	Yemen
D5	Clay	Morocco
D6	Clay	Saudi Arabia (Jeddah)
D7	Clay	Saudi Arabia (Makkah)
D8	Clay	Saudi Arabia (Bahrah)
D9	Ceramic	Turkey
D10	Ceramic	Vietnam
D11	Ceramic	Romania
D12	Ceramic	U.A.E
D13	Ceramic	Indonesia
D14	Ceramic	Portugal
D15	Ceramic	Thailand
D16	Ceramic	China
D17	Stone	Saudi Arabia (Jazan)
D18	Stone	Indonesia
D19	Stone	China
D20	Stone	Yemen

measured using a gamma spectrometry system with a high-purity germanium (HPGe) coaxial detector with a relative efficiency of 25% and a full width at half maximum (FWHM) of 2.0 keV at 1332 keV of ^{60}Co (Darko et al., 2012; Rajeshwari et al., 2014). The system was calibrated for energy and absolute efficiency, and all measurements were conducted for 10 h. The ^{232}Th concentration was determined from the average concentrations of ^{212}Pb (238.6 keV), ^{212}Bi (727.25keV), ^{212}Tl (583.1 keV), and ^{228}Ac (911.1 and 338.4 keV) in the samples, while the ^{214}Pb (351.9 and 295.09 keV) and ^{214}Bi (609.3, 1120.27, and 1764.5 keV) decay products were used to determine the average concentrations of ^{226}Ra. The average concentrations of ^{40}K and ^{137}Cs were determined through 1460.3 keV and 661.66 keV energy photopeaks, respectively. The radioactivity concentration C of these radionuclides was calculated using the following formula (Beretka and Mathew, 1985):

$$C \ (\text{Bq kg}^{-1}) = A_a / \varepsilon P_r w \tag{1}$$

where A_a is the intensity of gamma-line in a radionuclide (counts per second), ε is the efficiency for each gamma-ray line observed for the same number of channels for the sample or the background, P_r is the absolute transition probability of the gamma-ray decay, and w is the weight in kilograms of the sample.

RESULTS AND DISCUSSION

The activity concentrations of ^{226}Ra, ^{232}Th, and ^{40}K in the household cooking dishes were determined by using a HPGe detector, and the results are summarized in Table 2. The highest average activity concentrations of ^{226}Ra

Table 2. Activity levels of ^{226}Ra, ^{232}Th, ^{40}K, and Ra$_{eq}$ in household cooking dishes in Saudi Arabia.

Sample code	Activity concentration (Bq kg^{-1})			
	^{226}Ra	^{232}Th	^{40}K	^{137}Cs
D1	32.68±0.40	63.49±0.71	224.78±3.19	BDL
D2	37.16±1.03	65.41±1.68	562.69±0.67	0.70±0.10
D3	62.71±1.34	72.01±1.94	420.16±4.25	1.163±0.14
D4	45.26±1.10	58.58±0.86	400.49±3.70	2.68±0.16
D5	35.72± 0.92	52.68±0.82	500.674±7.22	0.94±0.13
D6	35.97±1.01	70.21±1.70	185.76±2.91	0.46±0.11
D7	14.52±0.25	18.80±0.51	284.56±3.04	0.47±0.08
D8	45.80±1.09	103.13±3.20	43.92±2.21	0.93±0.13
D9	38.53±0.80	48.65±1.27	470.389±3.28	0.48±0.79
D10	101.17±0.87	75.14±0.99	386.97±3.06	1.72±0.11
D11	58.31±0.95	65.84±2.70	656.96±6.63	0.96±0.12
D12	109.97±1.23	94.93±1.260	132.53±2.14	2.03±0.15
D13	43.66±0.85	87.83±1.26	455.25±3.14	0.71±0.08
D14	112.04± 0.89	72.82±1.91	429.68±3.02	1.89±0.13
D15	35.85±0.74	46.79±2.20	584.91±4.68	0.51±0.12
D16	192.35±2.01	192.41±1.97	457.73±4.04	3.12±0.19
D17	22.83±0.78	24.21±1.13	381.85±3.50	3.17±0.05
D18	9.32±0.53	9.78±1.13	131.20±1.59	BDL
D19	17.09±0.64	28.31±0.65	523.10±3.58	BDL
D20	5.75±0.43	6.17±0.48	103.81±2.08	BDL

BDL, below detectable limit.

and ^{232}Th were found in ceramic sample D16 (from China), with values of 192.35 and 192.41 Bq kg^{-1}, respectively. The lowest average activity concentrations of ^{226}Ra and ^{232}Th were found in stone sample D20 (from Yemen), with values of 4.12 and 4.85 Bq kg^{-1}, respectively. Ceramic sample D11 (from Romania) had the highest average activity concentrations of ^{40}K, 656.96 Bq kg^{-1}, and the lowest ^{40}K value was found in clay sample D8 manufactured in Bahrah, Saudi Arabia, with value of 43.92 Bq kg^{-1}. Ten samples (D2, D3, D5, D9, D11, D13, D14, D15, D16 and D19) exceeded the recommended limit of ^{40}K recommended limit of ^{40}K (UNSCEAR, 2008; Sahar and Naji, 2013) as shown in Figure 1. The highest activity concentration of ^{137}Cs was 3.17 Bq kg^{-1} from stone sample D17. Cesium 137 was not detected in four samples (Table 2): clay sample D1 imported from Egypt and stone samples D18, D19, and D20 imported from Indonesia, China, and Yemen, respectively. Table 2 shows that the concentrations of ^{226}Ra and ^{232}Th in clay and ceramic household cooking dishes exceeded world average values [(UNSCEAR], 2008; Marocchi et al., 2011; Mehra and Bala, 2014), with the exception of clay sample D7 manufactured in Makkah, Saudi Arabia. None of the stone samples exceeded the recommended limit for ^{226}Ra and ^{232}Th as shown in Figures 2 and 3.

Radium equivalent activity, Ra$_{eq}$

To evaluate the potential health effects of gamma radiation associated with using cooking dishes made from clay, ceramic, and stone, the radium equivalent activity index (Ra$_{eq}$) was determined by using the following expression (Beretka and Mathew, 1985):

$$Ra_{eq} (Bq\ kg^{-1}) = C_{Ra} + 1.43 C_{Th} + 0.077 C_k \qquad (2)$$

where C_{Ra}, C_{Th}, and C_K are the activity concentrations of ^{226}Ra, ^{232}Th, and ^{40}K in becquerels per kilogram, respectively. The range of measured Ra$_{eq}$ was 48.79–198.04 Bq kg^{-1} in clay samples, 144.31–502.74 Bq kg^{-1} in ceramic samples, and 22.56–97.85 Bq kg^{-1} in stone samples. All Ra$_{eq}$ values for the cooking dish samples were lower than the safety limit value of 370 Bq kg^{-1}, except for ceramic sample D16 from China (Ademola, 2009; Saleh and Abu Shayeb, 2014). The Ra$_{eq}$ values are listed in Table 3.

Absorbed dose rate, in air D$_R$ (nGy h^{-1})

Calculating the gamma absorbed dose rate in air is important because it is the first step in evaluating the
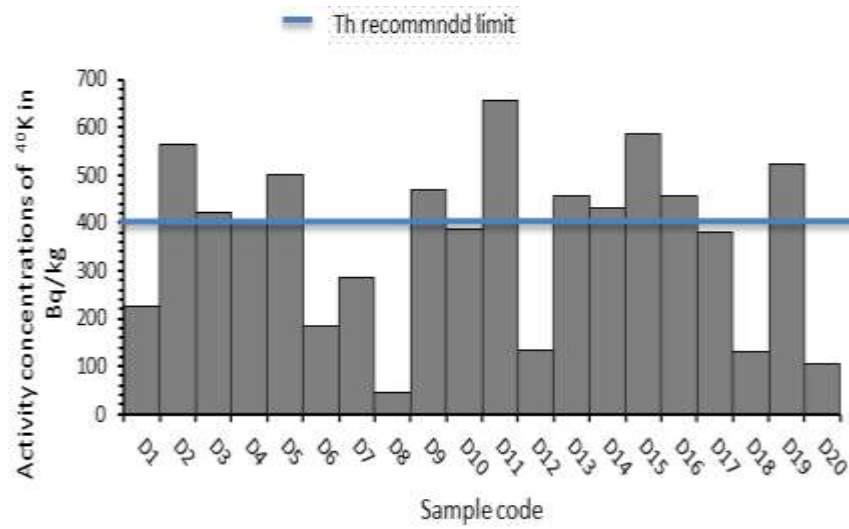
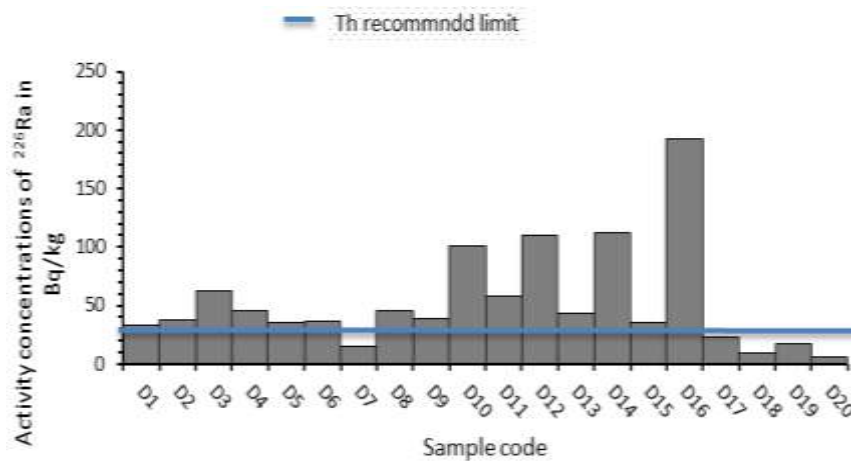**Figure 1.** Activity concentrations of ^{40}K in samples.

Figure 2. Activity concentrations of ^{226}Ra in samples.
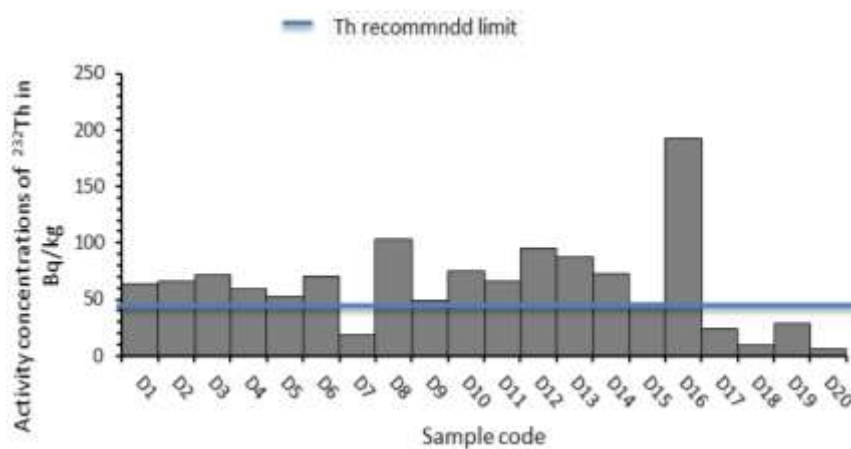

Figure 3. Activity concentrations of ^{232}Th in samples.

Table 3. Radium equivalent activity (Ra_{eq}), air-absorbed dose rate (D_R), annual effective dose rate (AEDE), annual gonadal dose equivalent (AGDE), external hazard (H_{ex}), and activity index (I_γ) in household cooking dishes used in Saudi Arabia.

Sample code	Ra_{eq} (Bq kg^{-1})	D_R (nGy h^{-1})	AEDE$_{indoor}$ (mSv y^{-1})	AGDE (mSv y^{-1})	H_{ex}	I_γ
D1	140.57	62.730	0.31	0.44	0.38	0.50
D2	174.02	80.140	0.39	0.57	0.47	0.64
D3	198.04	89.990	0.44	0.63	0.54	0.71
D4	159.87	72.990	0.36	0.51	0.43	0.58
D5	149.60	69.200	0.34	0.49	0.41	0.55
D6	150.67	66.770	0.33	0.46	0.41	0.53
D7	48.790	23.220	0.11	0.17	0.04	0.05
D8	197.24	85.530	0.42	0.59	0.53	0.69
D9	144.31	66.800	0.33	0.47	0.39	0.53
D10	238.41	108.26	0.53	0.75	0.64	0.84
D11	203.05	94.100	0.46	0.66	0.55	0.74
D12	255.99	113.67	0.56	0.78	0.69	0.89
D13	204.31	92.210	0.45	0.65	0.55	0.74
D14	247.82	113.06	0.55	0.73	0.67	0.88
D15	147.80	69.210	0.34	0.49	0.40	0.55
D16	502.74	224.17	1. 10	1.54	1.36	1.76
D17	86.85	41.100	0.20	0.29	0.24	0.33
D18	33.41	15.680	0.08	0.11	0.09	0.12
D19	97.85	46.810	0.23	0.34	0.27	0.37
D20	22.56	10.710	0.05	0.08	0.06	0.09

health risk associated with the studied samples. The absorbed dose rate in air, D_R (nGy h^{-1}), was determined by using the specific activity concentrations (Bq kg^{-1}) and the conversion factors of 0.427, 0.623, and 0.043 nGy h^{-1} per Bq kg^{-1} of ^{226}Ra, ^{232}Th, and ^{40}K, respectively, according to UNSCEAR (2008). The total dose rate D_R was then calculated by the following equation (Tufail et al., 1992):

$$D_R \text{ (nGy h}^{-1}) = 0.427C_{Ra} + 0.623C_{Th} + 0.043C_K \qquad (3)$$

where C_{Ra}, C_{Th}, and C_K are the activity concentrations (Bq kg^{-1}) of ^{226}Ra, ^{232}Th, and ^{40}K, respectively, in the samples listed in Table 2. The calculated values of D_R are shown in Table 3. The highest D_R was 224.17 nG h^{-1} in ceramic sample D16, which was from China, and the lowest value of D_R was 10.71 nG h^{-1} in stone sample D20, which was from Yemen. All D_R values were over the international recommended limit (57 nGy h^{-1}) (UNSCEAR, 2000; Sowole, 2014), except for clay sample D7, which was manufactured in Makkah, Saudi Arabia, and all stone samples.

Annual gonadal dose equivalent (AGDE)

The annual gonadal dose equivalent (AGDE) associated with the specific activities of ^{226}Ra, ^{232}Th, and ^{40}K in household cooking dishes manufactured from clay, ceramic, and stone materials was calculated using the following formula (Augustine et al., 2014):

$$\text{AGDE (}\mu\text{Sv y}^{-1}) = 3.09C_{Ra} + 4.18C_{Th} + 0.314C_K \qquad (4)$$

The obtained AGDE values are listed in Table 3. The AGDE values varied from 0.08 to 1.54 mSv y^{-1}. The obtained values in all samples are higher than the world average of (300 μSv y^{-1}) (UNSCEAR, 2000) except in clay sample D7 and in all stone samples.

Annual effective dose (AEDE$_{indoor}$ or E$_{air}$)

The estimated annual effective dose equivalent received by an individual was calculated by using a conversion factor of 0.7 Sv Gy^{-1}, which is used to convert the absorbed rate to member effective dose equivalent with an outdoor occupancy of 20 and 80 % for indoors (UNSCEAR, 1993; Ajayi, 2009). The annual effective doses in (mSv y^{-1}) were determined from the following formula (Beretka and Mathew 1985):

$$E_{air} = D_R \text{ (nGy.h}^{-1}) \times 8760 \text{ (h.y}^{-1}) \times 0.7(\times (10^3 \text{ mSv / nGy } 10^9)) \times 0.8 \qquad (5)$$

Equation (5) can be simplified to the following:

$$AEDE_{indoor} \ (mSv.y^{-1}) = D_R \times 4.905 \times 10^{-3} \qquad (6)$$

E_{air} is the effective dose rate in air, $AEDE_{indoor}$. The values of D_R are given in Equation 3 for all investigated samples. The estimated annual effective dose rates in air are given in Table 3. None of the values obtained for the annual effective dose exceeded 1 mSv y^{-1}, except for sample D16. The individual effective dose limits for normal exposure in the general public is defined by the ICRP (2007).

External hazard index, H_{ex}

To limit the external gamma radiation dose from household cooking dishes to less than 1.5 mSv y^{-1}, the external hazard index H_{ex} was calculated by using the following equation (Lu et al., 2012):

$$H_{ex} = (C_{Ra}/370) + (C_{Th}/259) + (C_K/4810) \qquad (7)$$

where C_{Ra}, C_{Th}, and C_K are the activity concentrations (Bq kg^{-1}) of ^{226}Ra, ^{232}Th, and ^{40}K, respectively. For the safe use of household cooking dishes and a negligible radiation hazard, the values of H_{ex} should be lower than unity and the maximum value of Ra_{eq} must be less than 370 Bq kg^{-1}. The calculated values of H_{ex} for the studied materials ranged from 0.04 to 1.36 (Table 3). The H_{ex} values for all investigated samples, except for sample D17, were less than unity (Xhixha et al., 2013).

Activity index, I_γ

To estimate the radiation hazard associated with ^{226}Ra, ^{232}Th, and ^{40}K, the radioactivity level index I_γ was calculated by the following equation (NEA-OECD 1979; Szabó et al. 2013):

$$I_\gamma = (1/300)C_{Ra} + (1/200)C_{Th} + (1/3000)C_K \qquad (8)$$

Where C_{Ra}, C_{Th}, and C_K are the specific activities (Bq kg^{-1}) of ^{226}Ra, ^{232}Th, and ^{40}K, respectively. I_γ varied from 0.05 in sample D7 from Makkah, Saudi Arabia, to 1.76 in ceramic sample D16 from China (Table 3). The values for all investigated samples were below unity, corresponding to an annual dose range of 0.3 to 1 mSv y^{-1}, except those for sample D16.

Concentrations of chemical elements using EDXRF

Table 4 shows the average concentrations of 33 elements (in wt/wt%), which were determined by using an EDXRF spectrometer (Yu et al., 2002; Rácz et al., 2016) to test whether elements were above toxicity reference levels (Noli and Tsamos, 2016). Silicon, Sn, In, and Fe were detected in all investigated samples, with Si being predominant and ranging from 19.50% (D18 from Indonesia) to 80.22% (D9 from Turkey). Iron concentrations varied from 14.69% (D1) to 0.868% (D20). Tin and In concentrations fell within the range of 0.0079% (D18) to 0.162% (D3) and 0.0077% (D18) to 0.0530% (D11), respectively, which exceeded the Sn and In concentrations in soil calculated by Kabata-Pendias and Mukherjee (2007). Egyptian clay sample D1 contained the highest amount of Fe (14.69%) and Yemeni stone sample D20 contained the lowest concentration (0.868%). The Fe concentrations in the samples exceeded the mean concentration (37,200 mg/kg) obtained by Towett et al. (2013), with the exception of samples D9, D10, D11, D12, D13, D14, D18, and D20.

Fourteen samples contained Ba exceeding the concentrations reported by Kabata-Pendias and Mukherjee (2007), and one sample was within the reference limit. Elements Th and U were detected in samples D11, D12, D14, D16, and D20 and in samples D5, D9, D10, D13, D14, D16, and D20, respectively, but not in the remaining samples. Potassium was found in all samples, except for D8, D11, D17, and D18. The K concentrations varied between 0.86% (D12) and 6.45% (D9), and except for samples D6 and D12, they exceeded the values reported by Kabata-Pendias and Mukherjee (2007). Calcium concentrations ranged from 1.16% (stone sample D20 from Yemen) to 33.16% (ceramic sample D10 from Vietnam). All samples contained Ca, except for samples D3, D5, D9, D14, and D16, and some (D4, D6, D8, D11, D12, D13, D17, and D20) contained Ca below the mean concentration (69,600 mg/kg) calculated by Towett et al. (2013). The Mg level in the present study varied between 6.07% (60,700 mg/kg) in the clay sample D5 from Morocco and 32.18% (321,800 mg/kg) in the stone sample D17 from Jazan, Saudi Arabia. Both of these values were considerably higher than 17700 mg/kg, the mean Mg concentration reported by Towett et al. (2013). Similarly, Al was found at the highest value of 24.68% (246,800 mg/kg) for clay sample D3 imported from Spain and the lowest concentration in ceramic sample D16 with a value of 1.56% (15,600 mg/kg). Seventeen samples contained Al, all of which exceed the mean concentration of Al in soil, with the exception of D16. Sodium was detected in six samples (D4, D12, D13, D17, D18, and D20), which exceeded the mean Na concentration of 16,000 mg/kg in soil reported by Towett et al. (2013). In the current study, the Na concentration ranged from 45.69% (456,900 mg/kg) in clay sample D4 imported from Yemen to 12.97% (129,700 mg/kg) in stone sample D17 locally made in Jazan, Saudi Arabia. Zirconium (Zr), Mo, Rh, Ru, Sb, Nb, Zn and Ni were found in some samples. In comparison

Table 4. Elements concentrations (in %, weight percent) using EDXRF analyzer.

Code	Na	Si	Mg	Al	Ca	K	Fe	Cl	Pd	Cu	Ba
D1	-	40.49±2.40	15.15±2.56	12.25±3.15	11.66±0.69	1.73±0.34	14.69±0.87	-	-	-	0.205±0.048
D2	-	33.62±2.35	25.61±2.43	17.34±2.68	7.38±0.52	3.43±0.36	9.62±0.67	-	-	-	0.336±0.051
D3	-	33.29± 1.40	25.04 ±1.99	24.68± 2.47	-	2.16± 0.73	7.90 ±0.25	-	-	-	0.26 ± 0.12
D4	45.69±4.88	24.26±1.88	9.32±1.55	7.11 ±1.45	3.49± 0.27	1.77± 0.23	6.60±0.51	-	-	-	-
D5	-	64.23±1.81	6.07 ±1.97	14.65± 2.13	-	3.87 ±0.48	8.79± 0.25	-	-	-	0.182± 0.025
D6	-	39.77±1.60	21.29±1.56	17.98±2.08	5.13±0.45	1.19±0.25	11.78±0.47	-	-	-	0.218±0.036
D7	-	30.49±1.42	26.92±2.17	16.24±2.61	9.24±0.46	2.45± 0.40	12.89±0.42	-	-	-	-
D8	-	47.8± 0.94	18.08±2.37	18.33±3.08	5.21± 0.35	-	6.01±0.13	--	-	-	0.515±0.056
D9	-	80.22±1.43	-	10.97± 2.99	-	6.45 ±0.68	1.76 ±0.07	--	-	0.058±0.027	-
D10	-	26.64±1.57	-	17.14 ± 1.75	33.16 ±1.61	3.02 ± 0.51	1.29 ± 0.07	1.64 ± 0.77	-	-	0.172 ± 0.069
D11	-	36.33± 3.73	20.78 ± 2.52	22.58± 3.42	2.87 ± 0.37	-	1.47± 0.15	-	0.039±0.016	-	3.28± 0.34
D12	18.97±6.89	62.13 ± 2.07	-	-	4.01± 0.30	0.86 ± 0.28	1.66 ± 0.06	-	-	0.141± 0.048	1.90± 0.10
D13	21.41±4.64	69.88 ± 1.63	-	-	2.69± 0.44	4.05 ± 0.40	1.00 ± 0.05	-	-	-	-
D14	-	77.04± 2.59	-	9.72 ±3.89	-	5.28 ± 0.50	3.21±0.11	-	-	-	0.157±0.072
D15	-	34.36±0.78	16.74±1.12	10.31±1.44	16.86± 0.25	2.71±0.29	10.20±0.19	-	-	-	0.117± 0.044
D16	-	72.14± 1.10	-	1.56 ± 2.59	-	4.87 ± 0.52	3.83 ±0.10	-	-	-	3.97±0.12
D17	12.97±4.28	37.20±0.91	32.18±0.92	6.79±0.79	2.56±0.30	-	7.07±0.18	-	-	-	0.067±0.029
D18	20.51 ± 3.26	19.50 ±0.67	23.27±0.83	18.74 ±0.65	14.33 ±0.49	-	3.19± 0.11	-	-	-	-
D19	-	37.79± 0.99	18.51±1.68	15.62±1.90	9.59± 0.42	5.54± 0.34	9.72±0.22	-	-	0.145±0.042	0.81±0.10
D20	29.42±3.46	56.46±1.04	-	6.03±2.76	1.16 ± 0.26	2.35 ±0.24	0.868±0.043	-	-	-	1.20 ± 0.05

Code	Rb	Pb	Cr	P	Y	S	Hf	Bi	Ni	Th	U
D1	-	-	-	-	-	-	-	-	0.111±0.035	-	-
D2	-	0.120±0.044	-	2.07±0.91	-	-	-	-	0.071±0.032	-	-
D3	-	1.87± 0.11	-	-	-	-	-	0.77 ± 0.13	-	-	-
D4	-	-	-	-	-	-	-	-	0.058± .026	-	-
D5	-	-	-	-	-	-	-	-	0.058±0.019	-	0.051±0.014
D6	-	-	-	-	-	-	-	-	0.095±0.024	-	-
D7	-	-	-	-	-	-	-	-	0.099±0.049	-	-
D8	-	-	-	-	-	-	-	-	-	-	-
D9	0.070± 0.019	-	0.093± 0.041	-	-	-	-	-	-	-	0.234±0.028
D10	0.040 ± 0.015	-	0.164 ± 0.03	10.29 ± 2.48	-	5.21 ±1.52	0.264±0.079	-	-	-	0.129 ± 0.025
D11	-	-	-	-	-	-	-	-	-	3.54 ± 0.51	-
D12	-	-	0.201±0.06	-	-	-	-	-	-	4.91± 0.23	-
D13	0.045± 0.012	-	-	-	-	-	-	-	-	-	0.152± 0.016
D14	0.057± 0.022	-	-	-	-	-	0.49±0.11	-	-	0.97 ± 0.11	0.224±0.033
D15	-	3.64±0.12	-	-	0.146±0.043	-	-	2.60±0.09	-	-	-

Table 4. Contd.

D16	0.047 ± 0.022	-	-	-	-	-	-	-	-	1.49 ± 0.13	0.179 ± 0.034
D17	-	-	0.206±0.068	-	-	-	-	-	0.194 ± 0.021	-	-
D18	-	-	-	-	-	-	-	-	-	-	-
D19	-	-	-	-	-	-	-	-	-	-	-
D20	-	-	-	-	-	-	-	-	-	0.815±0.06	0.033 ± 0.015

	Sn	In	Mo	Nb	Ru	Sb	Rh	Zr	Zn	Ti	Sr
D1	0.0147±0.0029	0.0185±0.0017	0.0370±0.0087	0.0562±0.0054	0.0138±0.0042	0.0124±0.0043	0.0091±0.0039	0.207±0.023	0.124±0.017	3.10±0.19	0.112±0.013
D2	0.0115±0.0028	0.0125±0.0014	0.0184±0.0087	0.0307±0.0069	0.0102±0.0037	0.0193±0.0040	-	-	-	-	0.154±0.012
D3	0.162±0.016	0.0314±0.0046	-	0.060±0.022	-	0.023±0.011	-	0.562± .077	-	1.42 ±0.12	-
D4	0.0084± 0.0025	0.0086± 0.0013	-	0.0324± 0.0075	-	-	-	0.065± 0.020	-	1.25 ± 0.10	0.020± 0.010
D5	0.0097± 0.0014	0.0105± 0.0007	0.0133± 0.0049	0.0239± 0.0042	0.0089± 0.0019	0.0065± 0.0021	-	0.044±0.010	0.089±0.010	1.87± 0.07	0.0212± 0.0058
D6	0.0113±0.002	0.0147±0.0011	0.0254±0.0073	0.0424±0.0043	0.0098±0.0032	0.0085±0.0030	-	0.181±0.017	0.164±0.012	2.01±0.19	0.0738±0.0099
D7	0.0193±0.0054	0.0258±0.0027	0.0411± 0.0090	0.0582±0.0097	0.0174±0.0080	-	-	-	-	1.13±0.26	0.136±0.024
D8	0.0180 ± 0.0032	0.0191± 0.0016	0.035± 0.014	0.0670± 0.0068	0.0110±0.0051	0.0110 ± 0.0047	0.0090± 0.0044	0.388± 0.027	0.242±0.017	3.17±0.28	0.071 ± 0.012
D9	0.0309± 0.0041	0.0312± 0.0021	-	0.044±0.016	0.0225±0.0056	0.0188 ± 0.0063	-	-	-	-	-
D10	0.0185±0.0037	0.0162±0.0028	-	0.031 ±0.014	-	-	-	-	0.540± 0.038	-	0.220 ± 0.013
D11	0.046±0.015	0.0530±0.0086	-	-	-	-	0.047±0.018	8.47 ± 0.87	0.232 ± 0.056	-	-
D12	0.0317 ± 0.0054	0.0377 ± 0.0028	-	-	-	0.0232±0.0078	-	4.81± 0.20	0.234±0.030	-	0.071± 0.026
D13	0.0212± 0.0022	0.0168± 0.0011	-	0.0260 ±0.0094	0.0126± 0.0031	0.0113 ± 0.0033	-	0.125±0.014	0.185 ± 0.015	0.373±0.023	-
D14	0.0622±0.0037	0.0324 ±0.0020	-	0.048±0.024	-	0.0200±0.0057	-	1.10 ± 0.05	1.12±0.05	0.68 ±0.14	-
D15	0.0274±0.0034	0.0209±0.0016	0.0312±0.0043	0.030±0.012	0.0138±0.0042	0.0686± 0.0042	-	-	-	1.98±0.08	0.051±0.013
D16	0.0350± 0.0066	0.0374± 0.0037	-	0.080 ± 0.029	-	0.0232± 0.0078	-	1.59± 0.08	0.173± 0.021	-	-
D17	0.0083±0.0016	0.0105±0.0008	0.0166±0.0021	0.0236±0.0026	0.0077±0.0022	0.0049±0.0024	0.0046±0.0021	-	-	0.631±0.053	0.0699± 0.0048
D18	0.0079 ± 0.0027	0.0077± 0.0020	0.0162 ± 0.0040	0.0220 ±0.0047	-	0.0072± 0.0028	-	-	-	0.236±0.076	0.0700±0.0060
D19	0.0244±0.0053	0.0258±0.0027	0.041± 0.011	0.061±0.013	0.0187 ±0.0080	-	-	-	-	1.67± 0.32	0.303±0.023
D20	0.0140± 0.0027	0.0155±0.0014	-	-	-	0.0086±0.0038	-	0.839±0.042	0.071 ± 0.010	0.72±0.16	-

"-": not detected.

with the concentrations of these metals reported by Kabata-Pendias and Mukherjee (2007), Zr, Mo, Rh, Ru, Sb, Nb, Zn and Ni were higher. The elements Cl, Pd, Cu, Rb, Pb, Cr, P, Y, S, Hf, and Bi were not detected in almost all samples. The concentrations of additional elements analyzed in the present study including Cl, Pd, Cu, Rb, Pb, Cr, P, Y, S, Hf, and Bi were also higher than the ranges reported by Kabata-Pendias and Mukherjee (2007). The content of Sr in the analyzed samples was higher than the range of 147 to 375 mg/kg obtained by Kabata-Pendias and Mukherjee (2007) except in sample D4 and D5. The maximum and minimum amounts were observed in sample D19, with a value of 0.303% (3030 mg/kg), and sample D4, with a value of 0.020% (200 mg/kg), respectively. Titanium was detected in 14 samples, with the concentration

varying from 0.236% (2360 mg/kg) in sample D18 to 3.17% (31,700 mg/kg) in sample D8. In comparison with the range 2900–15,480 mg/kg (Kabata-Pendias and Mukherjee, 2007), some samples in the current study had higher concentrations. In conclusion, attention must be paid to commercial marks and manufacturing country for the materials used in household cooking dishes.

Conclusion

Twenty samples of household cooking dishes in Saudi Arabia were analyzed for 33 chemical elements using ARL QUANT'X EDXRF. In addition, the natural radioactivity levels due to the presence of ^{40}K, ^{232}Th, and ^{226}Ra were determined using gamma spectrometry (HPGe). The concentrations of most elements exceeded the reference levels. The activity concentrations ranged between 14.52–62.71 Bq kg^{-1} in clay samples, 34.51–170.88 Bq kg^{-1} in ceramic samples, and 4.12–22.83 Bq kg^{-1} in stone samples for ^{226}Ra; 18.80–103.13 Bq kg^{-1} in clay samples, 46.79–164.17 Bq kg^{-1} in ceramic samples, and 4.85–28.31 Bq kg^{-1} in stone samples for ^{232}Th; and 43.92–562.69 Bq kg^{-1} in clay samples, 132.53–656.96 Bq kg^{-1} in ceramic samples, and 73.57–523.10 Bq kg^{-1} in stone samples for ^{40}K. The highest value of ^{137}Cs was 3.17 Bq kg^{-1}, which was found in a stone sample manufactured in Jazan, Saudi Arabia. All values for the radionuclides measured in the investigated samples were less than the world reference limit, with the exception of the ceramic sample from China. All values for the absorbed dose rate significantly exceeded the average value, except those associated with all stone samples and with the clay sample from Makkah, Saudi Arabia. The results indicate that these materials do not pose any significant radiological risk and they are safe for use in household cooking dishes.

Conflict of Interests

The authors have not declared any conflict of interests.

REFERENCES

Ademola JA (2009). Natural radioactivity and hazard assessment of imported ceramic tiles in Nigeria. Afr. J. Biomed. Res. 12(3):161–165.

Ajayi OS (2009). Measurement of activity concentrations of ^{40}K, ^{226}Ra and ^{232}Th for assessment of radiation hazards from soils of the southwestern region of Nigeria. Radiat. Environ. Biophys. 48:323-332.

Alharbi WR (2013). Natural radioactivity and dose assessment for brands of chemical and organic fertilizers used in Saudi Arabia. J. Mod. Phys. 4(1):344-348.

Amin SA, Naji M (2013). Natural radioactivity in different commercial ceramic samples used in Yemeni buildings. Radiat. Phys. Chem. 86:37–41.

Augustine KA, Bello AK, Adejumobi AC (2014). Determination of natural radioactivity and hazard in soil samples in and around gold mining area in Itagunmodi , south-western, Nigeria. J. Radiat. Res. Appl. Sci. 7:249-255.

Beretka J, Mathew PJ (1985). Natural radioactivity of Australian building materials, industrial wastes and by-products. Health Phys. 48:87-95.

Darko EO, Kpeglo DO, Akaho EHK, Chandorf CS, Adu PAS, Faanu A, Abankwah E, Lawluvi H, Awudu AR (2012). Radiation doses and hazards from processing of crude oil at the Tema oil refinery in Ghana. Radiat. Prot. Dosimetry 148(3):318-328.

El-Taher A (2012). Elemental analysis of granite by instrumental neutron activation analysis (INAA) and X-ray fluorescence analysis (XRF). Appl. Radiat. Isot. 70:350-354.

Faisal BMR, Haydar MA, Ali MI, Paul D, Majumder RK, Uddin MJ (2014). Assessment of natural radioactivity and associated radiation hazards in topsoil of Savar Industrial Area, Dhaka, Bangladesh. J. Nucl. Part. Phys. 4(4):129-136.

Guidotti L, Carini F, Rossi R, Gatti M, Cenci RM, Beone GM (2015). Gamma-spectrometric measurement of radioactivity in agricultural soils of the Lombardia region, northern Italy. J. Environ. Radioact. 142:36-44.

Hartyàni Z, Dávid E, Szabó S, Szilágyi V, Horváth T, Hargitai Tóth Á (2000). Determination of the trace elements distribution of polluted soils in Hungary by X-ray methods. Microchem. J. 67(1–3):195–200.

Hassan NM, Ishikawa T, Hosoda M, Sorimachi A, Tokonami S, Fukushi M, Sahoo SK (2010). Assessment of the natural radioactivity using two techniques for the measurement of radionuclide concentration in building materials used in Japan. J. Radioanal. Nucl. Chem. 283:15-21.

International Commission on Radiological Protection (ICRP) (2007). The 2007 Recommendations of the International Commission on Radiological Protection. ICRP Publication 103. Ann. ICRP 37:1-332.

Kabata-Pendias A, Mukherjee AB (2007). Trace Elements from Soils to Human. Springer-Verlag, Berlin.

Lu X, Yang G, Ren C (2012). Natural radioactivity and radiological hazards of building materials in Xianyang, China. Radiat. Phys. Chem. 81(7):780-784.

Marocchi M, Righi S, Bargossi GM, Gasparotto G (2011). Natural radionuclides content and radiological hazard of commercial ornamental stones: An integrated radiometric and mineralogical-petrographic study. Radiat. Meas. 46:538-545.

Mehra R, Bala P (2014). Assessment of radiation hazards due to the concentration of natural radionuclides in the environment. Environ. Earth Sci. 71:901–909.

Najam A, Younis SA, Kithah FH (2015). Natural radioactivity in soil samples in Nineveh Province and the associated radiation hazards. Int. J. Phys. 3(3):126-132.

Noli F, Tsamos P (2016). Concentration of heavy metals and trace elements in soils, waters and vegetables and assessment of health risk in the vicinity of a lignite-fired power plant. Sci. Total Environ. 563–564:377-385.

Nuclear Energy Agency, Organization for Economic Co-Operation and Development (NEA-OECD) (1979). Exposure to radiation from natural radioactivity in building materials. Report by NEA Group of Experts. OECD, Paris, France.

Rácz L, Solti S, Gresits I, Tölgyesi S, Benedek D, Valentínyi N, Mizsey P (2016). Measurement of rarely investigated trace elements As, P, Sr, Zr, Rb and Y in waste tires. Period. Polytech. Chem. Eng. 60(2):78-84.

Rajeshwari T, Rajesh S, Kerur BR, Anilkumar S, Krishnan N, Pant AD (2014). Natural radioactivity studies of Bidar soil samples using gamma spectrometry. J. Radioanal. Nucl. Chem. 300:61-65.

Sahar AA, Naji M (2013). Natural radioactivity in different commercial ceramic samples used in Yemeni buildings. Radiat. Phys. Chem. 86:37–41.

Salas HT, Nalini HA Jr, Mendes JC (2006). Radioactivity dosage evaluation of Brazilian ornamental granitic rocks based on chemical data, with mineralogical and lithological characterization. Environ. Geol. 49:520–526.

Saleh H, Abu Shayeb M (2014). Natural radioactivity distribution of southern part of Jordan (Ma'an) soil. Ann. Nucl. Energy 65:184-189.

Sitko R, Zawisza B, Jurczyk J, Buhl F, Zielonka U (2004). Determination of high Zn and Pb concentrations in polluted soils using energy-dispersive X-ray fluorescence spectrometry. Polish J. Environ. Stud. 13(1):91-96.

Sowole O (2014). Assessment of radiological hazard indices from surface soil to individuals from major markets at Sagamu Ogun state, Nigeria. Sci. World J. 9(3):1-4.

Szabó Z, Völgyesi P, Nagy HÉ, Szabó C, Kis Z, Csorba O (2013). Radioactivity of natural and artificial building materials—A comparative study. J. Environ. Radioact. 118:64-74.

Towett EK, Shepherd KD, Cadisch G (2013). Quantification of total element concentrations in soils using total X-ray fluorescence spectroscopy (TXRF). Sci. Total Environ. 463–464:374–388.

Tufail M, Ahmad N, Almakky S, Zafar MS, Khan HA (1992). Natural radioactivity in the ceramics used in dwellings as construction material. Sci. Total Environ. 127:243-253.

United Nations Scientific Committee on the Effect of Atomic Radiation (UNSCEAR) (1993). Sources and effects of ionizing radiation. United Nations, New York.

United Nations Scientific Committee on the Effect of Atomic Radiation (UNSCEAR) (2000). Sources and effects of ionizing radiation. Report to general assembly, Annex B exposure from natural radiation sources. United Nations, New York.

United Nations Scientific Committee on the Effect of Atomic Radiation (UNSCEAR) (2008). Sources and effects of ionizing radiation. Report to general assembly, Annexes C,D and E B. sources and effects of ionization radiation, New York.

Xhixha G, Ahmeti A, Bezzon GP, Bitri M, Broggini C, Buso GP, Caciolli A, Callegari I, Cfarku F, Colonna T, Fiorentini G, Guastaldi E, Mantovani F, Massa G, Menegazzo R, Mou L, Prifti D, Rossi Alvarez C, Sadiraj Kuqi DH, Shyti M, Tushe L, Xhixha Kaçeli M, Zyfi A (2013). First characterization of natural radioactivity in building materials manufactured in Albania. Radiat. Prot. Dosim. 155(2):217-223.

Yu KN, Yeung ZLL, Lee LYL, Stokes MJ, Kwok RCW (2002). Determination of multi-element profiles of soil using energy dispersive X-ray fluorescence (EDXRF). Appl. Radiat. Isot. 57:279-284.

International Journal of Physical Sciences

academicJournals